Peer-reviewed version available at *Nanomaterials* **2019**, *9*, 1554; doi:10.3390/nano9111554

Article

DC Self-Field Critical Current in Superconductor/Dirac-Cone Material/Superconductor Junctions and The Request for Ballistic Model Reexamination

Evgueni F. Talantsev [1,2,*]

[1] M. N. Mikheev Institute of Metal Physics, Ural Branch, Russian Academy of Sciences, 18, S. Kovalevskoy St., Ekaterinburg, 620108, Russia; evgeny.talantsev@imp.uran.ru
[2] NANOTECH Centre, Ural Federal University, 19 Mira St., Ekaterinburg, 620002, Russia; evgeny.talantsev@urfu.ru
* Correspondence: evgeny.talantsev@imp.uran.ru; Tel.: +007-912-676-0374

Abstract: Recently, several research groups have reported on anomalous enhancement of the self-field critical currents, $I_c(sf,T)$, at low temperatures in superconductor/Dirac-cone material/superconductor (S/DCM/S) junctions. Some papers attributed the enhancement to the low-energy Andreev bound states arising from winding of the electronic wave function around DCM. In this paper, $I_c(sf,T)$ in S/DCM/S junctions have been analyzed by two approaches: modified Ambegaokar-Baratoff and ballistic Titov-Beenakker models. It is shown that the ballistic model is an inadequate tool to analyze experimental data from S/DCM/S junctions. The primary mechanism for limiting superconducting current in S/DCM/S junctions is different from the conventional view that the latter is the maximum value within the order parameter phase variation. Thus, there is a need to develop a new model for self-field critical currents in S/DCM/S systems.

Keywords: the self-field critical current; induced superconductivity in Dirac-cone materials; single layer graphene; multiple-band superconductivity

1. Introduction

Intrinsic superconductors [1] of rectangular cross-section (with width $2a$ and thickness $2b$) exhibit non-dissipative transport self-field critical current, $I_c(sf,T)$ (i.e., when no external magnetic field applies), which is given by the following universal equation [2-4]:

$$I_c(sf,T) = \frac{\phi_0}{\pi\cdot\mu_0}\cdot\left[\frac{ln(1+\sqrt{2}\cdot\kappa_c)}{\lambda_{ab}^3(T)}\cdot\left(\frac{\lambda_c(T)}{b}\cdot\tanh\left(\frac{b}{\lambda_c(T)}\right)\right)+\frac{ln(1+\sqrt{2}\cdot\gamma(T)\cdot\kappa_c)}{\sqrt{\gamma(T)}\cdot\lambda_{ab}^3(T)}\left(\frac{\lambda_{ab}(T)}{a}\tanh\left(\frac{a}{\lambda_{ab}(T)}\right)\right)\right]\cdot(a\cdot b), \qquad (1)$$

where $\phi_0 = 2.067\cdot10^{-15}\ Wb$ is the magnetic flux quantum, $\phi_0 = 4\cdot\pi\cdot10^{-7}\ H/m$ is the magnetic permeability of free space, $\lambda_{ab}(T)$ and $\lambda_c(T)$ are the in-plane and out-of-plane London penetration depths respectively, $\kappa_c = \lambda_{ab}(T)/\xi_{ab}(T)$, $\xi_{ab}(T)$ is the in-plane coherence length, and $\gamma(T) = \lambda_c(T)/\lambda_{ab}(T)$ is the electron mass anisotropy. It was shown, that Eq. 1 quantitatively and accurately describes $I_c(sf,T)$ in more than 100 superconductors, ranging from elemental Zn with $T_c = 0.65$ K to highly-compressed H_3S with $T_c \gtrsim 200\ K$ [2-4], and samples dimensions from several Å to about 1 mm [5].

All intrinsic superconductors [1] can induce superconducting state in non-superconducting materials by the Holm-Meissner effect [6]. However, a universal equation for non-dissipative self-field critical transport current, $I_c(sf,T)$, in superconductor/non-superconductor/superconductor junctions is still unknown. Ambegaokar and Baratoff (AB) [7,8] were the first who proposed an equation for $I_c(sf,T)$ in superconductor/insulator/superconductor (S/I/S) systems. Later, Kulik and

Preprints (www.preprints.org) | NOT PEER-REVIEWED | Posted: 27 September 2019 doi:10.20944/preprints201909.0307.v1

Peer-reviewed version available at Nanomaterials 2019, 9, 1554; doi:10.3390/nano9111554

Omel'yanchuk (KO) [9-11] proposed two models for different types of superconductor/normal conductor/superconductor junctions (which are known as KO-1 [9] and KO-2 [10]).

In general, S/N/S junctions are classified by the comparison of the device length (L) to two characteristic length scales of the junction, which are the mean free path of the charge carriers, l_e, and the superconducting correlation length, ξ_s. These length scales classify whether the junction is in short ($L \ll \xi_s$) or long (i.e., $L \gg \xi_s$) regime and ballistic ($L \ll l_e$) or diffusive ($L \gg l_e$) limit, respectively.

For about one decade the KO-1 model was considered to be the primary model to describe $I_c(sf,T)$ in superconductor/graphene/superconductor (S/G/S) junctions (a detailed review of different models for $I_c(sf,T)$ in S/G/S junctions was given by Lee and Lee [12]). However, recent technological progress in fabricating high-quality S/G/S junctions demonstrates a large difference between the KO-1 model and experimental $I_c(sf,T)$ data [13]. Detailed discussion of all models, including a model by Takane and Imura [14], which was proposed to describe $I_c(sf,T)$ in superconductor/Dirac-cone material/superconductor (S/DCM/S) junctions is given by Lee and Lee [12].

It should be noted that a universal quantitatively accurate equation for critical currents at applied magnetic field, B, is unknown to date as for intrinsic superconductors [15-19], as for Josephson junctions [12,20,21]. The discussion of these important problems, as well as the discussion of interface superconductivity [22-24] and generic case of two-dimensional (2D) superconductivity [25-49], is, however, beyond the scope of this paper.

The primary task for this work is to show that $I_c(sf,T)$ in a variety of S/DCM/S junctions in the ballistic regime cannot be described by KO-based model. To prove this, experimental $I_c(sf,T)$ datasets in S/DCM/S junctions were analyzed by two models: modified Ambegaokar-Baratoff model [51] and ballistic Titov-Beenakker model [52].

It needs to be noted, that some S/DCM/S junctions show the $I_c(sf,T)$ enhancement at reduced temperature of $T \leq 0.25 \cdot T_c$. For instance, the enhancement in atomically-thin MoRe/single layer graphene (SLG)/MoRe junction was first reported by Calado *et al.* [53]. Raw experimental $I_c(sf,T)$ data reported by Borzenets *et al.* [54] in nominally the same MoRe/SLG/MoRe junctions also shows the enhancement at $T \leq 0.25 \cdot T_c$. Based on this, the $I_c(sf,T)$ enhancement at low reduced temperatures in Nb/BiSbTeSe$_2$-nanoribon/Nb reported by Kayyalha *et al.* [55] cannot be considered as an unique property of superconductor/topological insulator/superconductor (S/TI/S) junctions, but one is rather the demonstration of general feature of S/DCM/S devices and atomically thin superconducting systems. Also, it is important to mention that Kurter *et al.* [56] were the first who reported $I_c(sf,T)$ enhancement in S/TI-nanoribbon/S junction at reduced temperature of $T \leq 0.25 \cdot T_c$.

In the result of performed $I_c(sf,T)$ analysis in this paper, it has been shown that a new model is requested to describe dissipation-free transport currents in S/DCM/S junctions.

2. Models description

The amplitude of dissipation-free transport current, $I_c(sf,T)$, in S/I/S junction was first given by Ambegaokar and Baratoff (AB) [3,4]:

$$I_c(sf,T) = \frac{\pi \cdot \Delta(T)}{2 \cdot e \cdot R_n} \cdot tanh\left(\frac{\Delta(T)}{2 \cdot k_B \cdot T}\right), \quad (1)$$

where $\Delta(T)$ is the temperature-dependent superconducting gap, e is the electron charge, R_n is the normal-state tunneling resistance in the junction, and k_B is the Boltzmann constant. In work [50] it was proposed to substitute $\Delta(T)$ in Eq. 1 by analytical expression given by Gross *et al.* [57]:

$$\Delta(T) = \Delta(0) \cdot \tanh\left(\frac{\pi \cdot k_B \cdot T_c}{\Delta(0)} \cdot \sqrt{\eta \cdot \left(\frac{\Delta C}{C}\right) \cdot \left(\frac{T_c}{T} - 1\right)}\right), \quad (2)$$

where $\Delta(0)$ is the ground-state amplitude of the superconducting band, $\Delta C/C$ is the relative jump in electronic specific heat at the transition temperature, T_c, and $\eta = 2/3$ for s-wave superconductors [55]. In the result, T_c, $\Delta C/C$, $\Delta(0)$, and normal-state tunneling resistance, R_n, of the S/I/S junction, or in more general case of S/N/S junction, can be deduced by fitting experimental $I_c(sf,T)$ datasets to Eq. 1 for which the full expression is [51]:

Peer-reviewed version available at *Nanomaterials* **2019**, *9*, 1554; doi:10.3390/nano9111554

$$I_c(sf,T) = \frac{\pi\cdot\Delta(0)\cdot\tanh\left(\frac{\pi\cdot k_B\cdot T_c}{\Delta(0)}\cdot\sqrt{\eta\cdot\left(\frac{\Delta C}{C}\right)\cdot\left(\frac{T_c}{T}-1\right)}\right)}{2\cdot e\cdot R_n}\cdot tanh\left(\frac{\Delta(0)\cdot\tanh\left(\frac{\pi\cdot k_B\cdot T_c}{\Delta(0)}\cdot\sqrt{\eta\cdot\left(\frac{\Delta C}{C}\right)\cdot\left(\frac{T_c}{T}-1\right)}\right)}{2\cdot k_B\cdot T}\right), \quad (3)$$

It should be noted that direct experiments performed by Natterer *et al.* [58] showed that the superconducting gap does exist in graphene which is in proximity contact with superconducting electrodes. The gap amplitude, $\Delta(T)$, has characteristic decaying length [58], which is the expected behavior from primary idea of the proximity effect [6]. As a direct consequence of it, clear physical meaning remains for the relative jump in electronic specific heat at the transition temperature, $\Delta C/C$, due to this parameter is an essential thermodynamic consequence for the appearance of the superconducting energy gap, $\Delta(T)$. As it was shown in Ref. 51, $\Delta C/C$ is the fastest decaying parameter of the superconducting state in S/N/S junctions, over the junction length, L, while T_c is the most robust one.

In Ref. 51 it was shown that S/SLG/S and S/Bi_2Se_3/S junctions exhibit two-decoupled band superconducting state. Thus, for the general case of N-decoupled bands, the temperature-dependent self-field critical current, $I_c(\mathrm{sf},T)$, can be described by the equation:

$$I_c(sf,T) = \sum_{i=1}^{N}\frac{\pi\cdot\Delta_i(T)}{2\cdot e\cdot R_{n,i}}\cdot\theta\left(T_{c,i}-T\right)\cdot tanh\left(\frac{\Delta_i(T)}{2\cdot k_B\cdot T}\right), \quad (4)$$

where the subscript i refers to the i-band, $\theta(x)$ is the Heaviside step function, and each band has its own independent parameters of $T_{c,i}$, $\Delta C_i/C_i$, $\Delta_i(0)$, and $R_{n,i}$. Eqs. 4 was also used to analyze experimental $I_c(\mathrm{sf},T)$ data for several S/DCM/S junctions [59].

Titov and Beenakker [52] proposed that $I_c(\mathrm{sf},T)$ in S/DCM/S junction at the conditions near the Dirac point can be described by the equation:

$$I_c(sf,T) = 1.33\cdot\frac{e\cdot\Delta(T)}{\hbar}\cdot\frac{W}{\pi\cdot L}, \quad (5)$$

where W is the junction width. In this paper, analytical equation for the gap (Eq. 2 [57]) is substituted in Eq. 5:

$$I_c(sf,T) = 1.33\cdot\frac{e\cdot\Delta(0)\cdot\tanh\left(\frac{\pi\cdot k_B\cdot T_c}{\Delta(0)}\cdot\sqrt{\eta\cdot\left(\frac{\Delta C}{C}\right)\cdot\left(\frac{T_c}{T}-1\right)}\right)}{\hbar}\cdot\frac{W}{\pi\cdot L}, \quad (6)$$

with the purpose to deduce T_c, $\Delta C/C$, and $\Delta(0)$ values in the S/DCM/S junctions from the fit of experimental $I_c(\mathrm{sf},T)$ datasets to Eq. 5. For a general case of N-decoupled bands, temperature-dependent self-field critical current $I_c(\mathrm{sf},T)$ in S/DCM/S junctions can be described by the equation:

$$I_c(sf,T) = 1.33\cdot\frac{e}{\pi\cdot\hbar}\cdot\frac{W}{L}\cdot\sum_{i=1}^{N}\Delta_i(T)\cdot\theta\left(T_{c,i}-T\right), \quad (7)$$

Based on a fact that W and L can be measured with very high accuracies, Eq. 6 has the minimal, ever proposed, number of free-fitting parameters (which are T_c, $\Delta C/C$, $\Delta(0)$) to fit to the experimental $I_c(\mathrm{sf},T)$ dataset. However, as we demonstrate below, the ballistic model (Eq. 5 [52]) is not the most correct model to describe $I_c(\mathrm{sf},T)$ in S/DCM/S junctions. It should be noted, that Eq. 3 utilizes the same minimal set of parameters within BCS theory, i.e. T_c, $\Delta C/C$, $\Delta(0)$, to describe superconducting state in S/N/S junction and R_n as a free-fitting parameter to describe the junction.

It should be stressed that a good reason must be presented for requiring a more complex model than is needed to adequately explain the experimental data [60,61].

In the next section, Eqs. 3,4,6,7 will be applied to fit experimental $I_c(\mathrm{sf},T)$ datasets for a variety of S/DCM/S junctions with the purpose to reveal the primary superconducting parameters of these systems and to prove that the modified Ambegaokar and Baratoff model (Eqs. 3,4) [51,59] describes the superconducting state in S/DCM/S junctions with higher accuracy.

3. Results

3.1. Micrometer-long tantalum/graphene/tantalum (Ta/G/Ta) junctions

Preprints (www.preprints.org) | NOT PEER-REVIEWED | Posted: 27 September 2019 doi:10.20944/preprints201909.0307.v1

Peer-reviewed version available at Nanomaterials 2019, 9, 1554; doi:10.3390/nano9111554

Jang and Kim [62] reported experimental $I_c(sf,T)$ datasets and fit to KO-1 model (in their Fig. 2,d [62]) for micrometer long ballistic Ta/G/Ta junctions. The $I_c(sf,T)$ fit to KO-1 model (Fig. 2,d [62]) and deduced parameters are in disagreement with experimental values based on I_cR_n product. In our Fig. 1 we show $I_c(sf,T)$ datasets for Device 1 [62] (recorded at gate voltage V_g = 10 V) and fits to single-band ballistic model, Eq. 6 (in Fig. 1,a) and single-band modified AB model Eq. 3 (Fig. 1,b). Device 1 has W = 6 μm, L = 1 μm, and ξ_s = 16 μm [62]. This means that the ballistic limit of $L \ll \xi_s$ is satisfied for these junctions.

Deduced parameters from the fit to ballistic model (Eq. 6) in Fig. 1,a are in remarkable disagreement with any physical-backgrounded expectations, i.e. the ratio of $\frac{2\cdot\Delta(0)}{k_B\cdot T_c} = 22.7$ (which should be comparable with s-wave BCS weak coupling limit of $\frac{2\cdot\Delta(0)}{k_B\cdot T_c} = 3.53$) and $\frac{\Delta C}{C} = 17.7$ (which should be comparable with s-wave BCS weak coupling limit of $\frac{\Delta C}{C} = 1.43$).

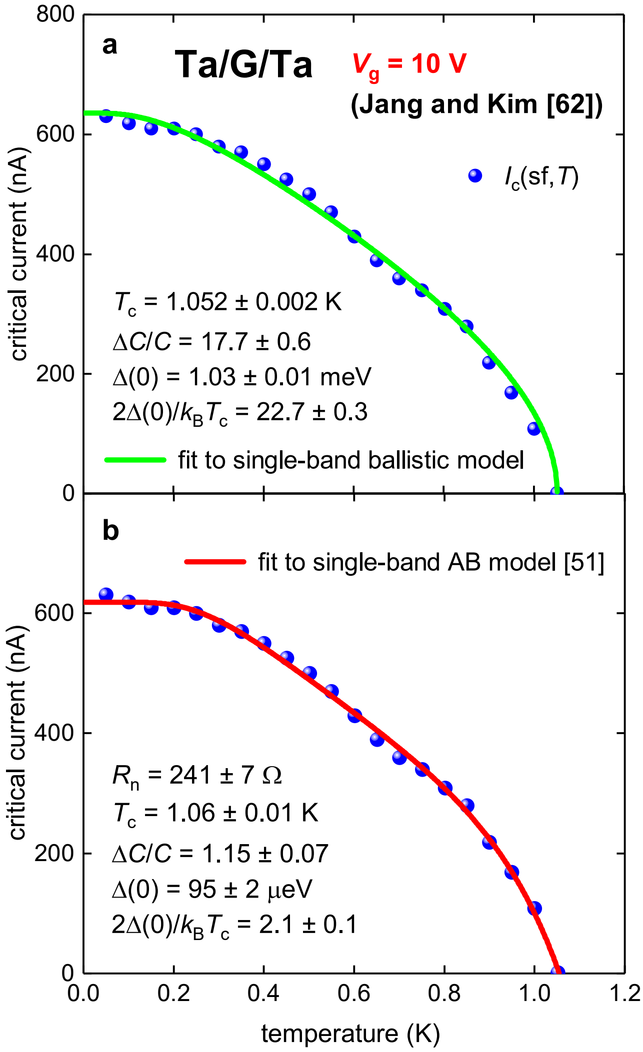

Figure 1. Experimental $I_c(sf,T)$ for Ta/G/Ta junction (Device 1) at gate voltage of V_g = 10 V [62] and data fits to single-band ballistic model (Eq. 6, Panel a) and single-band modified AB model (Eq. 3, Panel b) (**a**) Ballistic model. fit quality is R = 0.9948; (**b**) modified AB model [51] fit quality is R = 0.9980.

It needs to be noted that the highest experimental value for phonon-mediated superconductors of $\frac{2\cdot\Delta(0)}{k_B\cdot T_c} \approx 5$ was measured for lead- and bismuth-based alloys [63,64], and deduced value by the ballistic model $\frac{2\cdot\Delta(0)}{k_B\cdot T_c} \approx 23$ does not have physical interpretation.

In contract, the fit to Eq. 3 reveals superconducting parameters in expected ranges of $\frac{2\cdot\Delta(0)}{k_B\cdot T_c} = 2.1 \pm 0.1$ and $\frac{\Delta C}{C} = 1.15 \pm 0.07$, i.e. these parameters are slightly suppressed from s-wave BCS weak-

Preprints (www.preprints.org) | NOT PEER-REVIEWED | Posted: 27 September 2019 doi:10.20944/preprints201909.0307.v1

Peer-reviewed version available at Nanomaterials 2019, 9, 1554; doi:10.3390/nano9111554

coupling limits as expected [51,59]. It should also be noted, that free-fitting parameter R_n = 241 ± 7 Ω is in a good agreement with experimental measured value for this junction [62].

It can be seen (Fig. 1), that there is an upturn in experimental I_c(sf,T) at T ~ 0.65 K, which is a manifestation of the second superconducting band opening in this atomically thin S/N/S junction [51,59]. Thus, experimental I_c(sf,T) dataset was fitted to two-band models (Eqs. 7 and 4). Results of these fits are shown in Fig. 2.

The fit reveals a large disagreement of parameters deduced by ballistic model with expected values within frames for BCS theory. In contrast with this, deduced parameters by modified AB model [51,59] are within weak-coupling limits of BCS. As it was shown in Ref. 51, raw experimental I_c(sf,T) datasets should be reasonably dense to deduce parameters by AB model with small uncertainties.

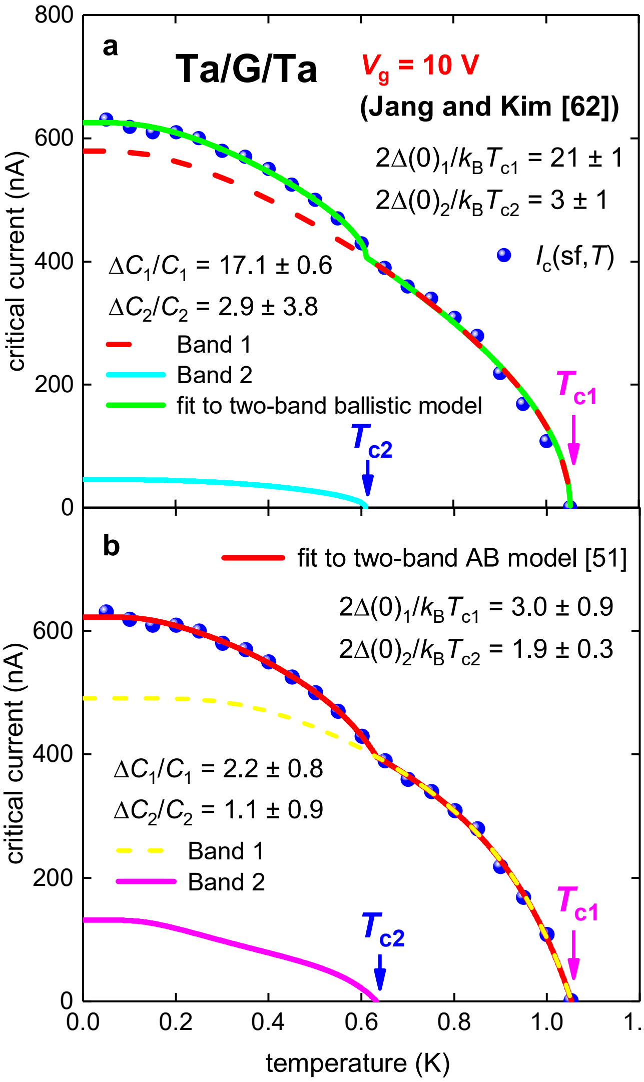

Figure 2. Experimental I_c(sf,T) for Ta/G/Ta junction (Device 1) at gate voltage of V_g = 10 V [62] and data fits to two-band ballistic model (Eq. 7, Panel a) and two-band modified AB model (Eq. 4, Panel b) (**a**) Ballistic model. Derived parameters: T_{c1} = 1.052 ± 0.001 K, T_{c2} = 0.61 ± 0.02 K, fit quality is R = 0.9978; (**b**) modified AB model [51] Derived parameters: R_{n1} = 429 ± 184 Ω, T_{c1} = 1.053 ± 0.003 K, $\Delta_1(0)$ = 134 ± 41 μeV, R_{n2} = 603 ± 209 Ω, T_{c2} = 0.63 ± 0.03 K, $\Delta_2(0)$ = 50 ± 8 μeV, fit quality is R = 0.9994.

3.2. Planar Nb/BiSbTeSe$_2$-nanoribbon/Nb junctions

Kayyalha *et al.* [55] reported I_c(sf,T) for five Nb/BiSbTeSe$_2$-nanopribbon/Nb junctions at different gate voltage, V_g. In this paper I_c(sf,T) datasets for Sample 1 at V_g = -20 V, 0 V and 45 V [55] are analyzed by two-band models (Eqs. 4 and 7), because it is already shown in Ref. 59, that these junctions exhibit

Preprints (www.preprints.org) | NOT PEER-REVIEWED | Posted: 27 September 2019 doi:10.20944/preprints201909.0307.v1

Peer-reviewed version available at *Nanomaterials* **2019**, *9*, 1554; doi:10.3390/nano9111554

two-band superconducting state. In Fig. 3 experimental $I_c(sf,T)$ dataset [55] and fits are shown. For this junction L = 40 nm [55], and ξ_s = 640 nm [55], and thus, ballistic regime, $L << \xi_s$, is well satisfied.

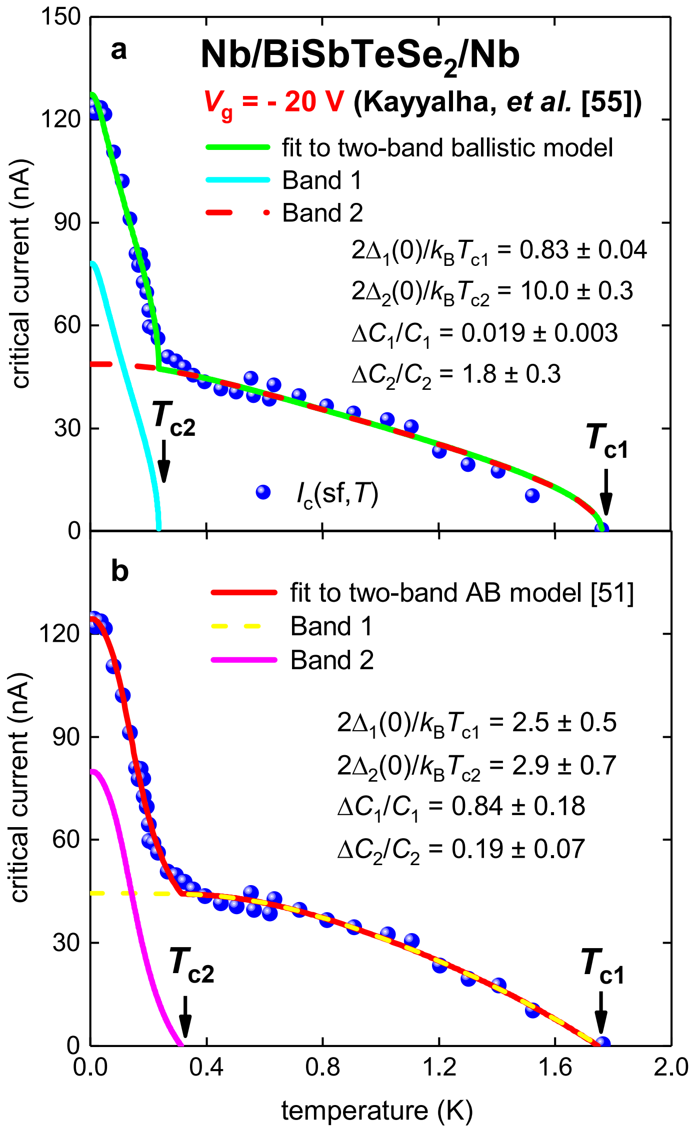

Figure 3. Experimental $I_c(sf,T)$ for Nb/BiSbTeSe$_2$-nanoribbon/Nb junction (Sample 1 [55]) at gate voltage V_g = - 20 V. (**a**) Ballistic model. Derived parameters: T_{c1} = 1.76 ± 0.01 K, $\Delta_1(0)$ = 63 ± 3 μeV, $\Delta C_1/C_1$ = 0.019 ± 0.003, $2\Delta_1(0)/k_BT_{c1}$ = 0.83 ± 0.04, T_{c2} = 0.236 ± 0.003 K, $\Delta_2(0)$ = 101 ± 4 μeV, $\Delta C_2/C_2$ = 1.8 ± 0.3, $2\Delta_2(0)/k_BT_{c2}$ = 10.0 ± 0.3, fit quality is R = 0.990; (**b**) Modified AB model [51]. Derived parameters: T_{c1} = 1.74 ± 0.04 K, $\Delta_1(0)$ = 190 ± 40 μeV, $\Delta C_1/C_1$ = 0.84 ± 0.18, $2\Delta_1(0)/k_BT_{c1}$ = 2.5 ± 0.5, R_{n1} = 6.7 ± 1.6 kΩ, T_{c2} = 0.31 ± 0.02 K, $\Delta_2(0)$ = 38.2 ± 9.7 μeV, $\Delta C_2/C_2$ = 0.19 ± 0.07, $2\Delta_2(0)/k_BT_{c2}$ = 2.85 ± 0.70, R_{n2} = 0.75 ± 0.18 kΩ, $\frac{T_{c2}}{T_{c1}}$ = 0.18 ± 0.02, fit quality is R = 0.9953.

Despite a fact that fits to both models have similar quality, deduced parameters of the superconducting state, i.e. $\Delta C_i/C_i$, $\Delta_i(0)$, and $\frac{2\cdot\Delta_i(0)}{k_B\cdot T_{c,i}}$, for the case of the ballistic models (Fig. 3,a), similar to the case of Ta/G/Ta junction (Figs. 1,2), are remarkably different from expected values expected from BCS theory. Also, there is two orders in magnitude difference between deduced $\Delta C_i/C_i$ for two bands for the same sample, and one order of magnitude for $\frac{2\cdot\Delta_i(0)}{k_B\cdot T_{c,i}}$ which are unavoidable evidences that the ballistic model needs to be reexamined. In contrast with this, the fit to modified AB model [51] (Fig. 3,b) reveals deduced parameters, including R_{ni} values, in expected ranges. It should be noted

Preprints (www.preprints.org) | NOT PEER-REVIEWED | Posted: 27 September 2019 doi:10.20944/preprints201909.0307.v1

Peer-reviewed version available at Nanomaterials 2019, 9, 1554; doi:10.3390/nano9111554

that full analysis (within modified AB model [51]) of I_c(sf,T) datasets in junctions reported by Kayyalha *et al.* [55] can be found elsewhere [59].

In Fig. 4 experimental I_c(sf,T) dataset [55] and fits to two models for Sample 1 at gate voltage V_g = 0 V also demonstrate that the ballistic model is an inadequate tool to analyze experimental data in S/DCM/S junctions.

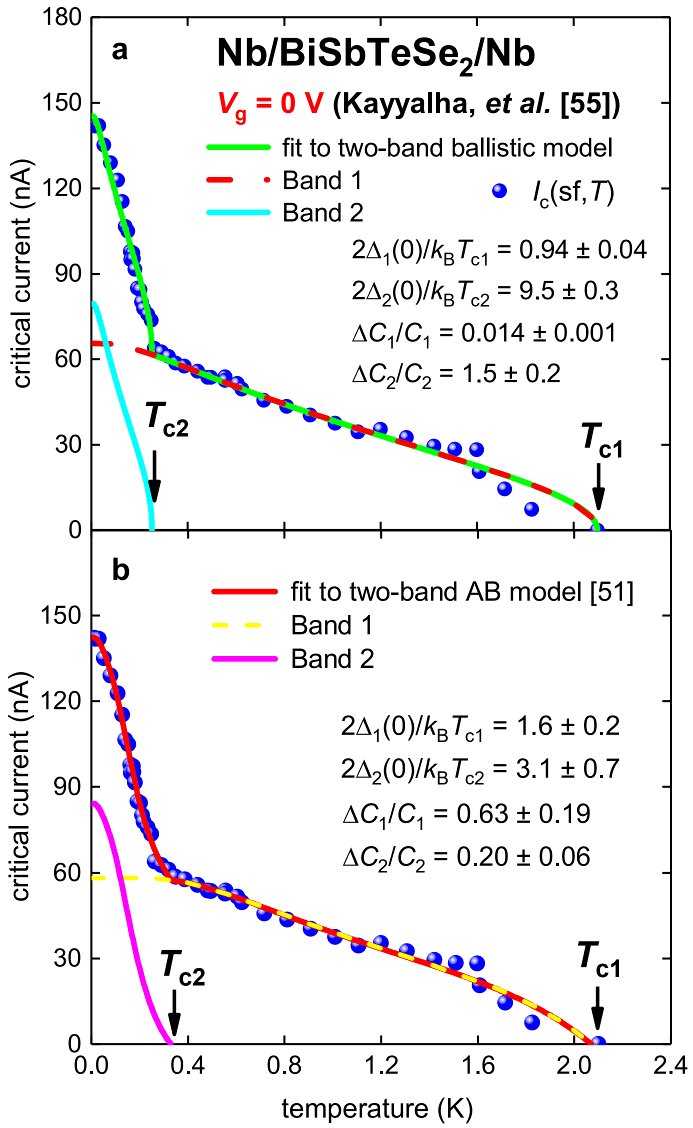

Figure 4. Experimental I_c(sf,T) for Nb/BiSbTeSe_2-nanoribbon/Nb junction (Sample 1 [55]) at gate voltage V_g = 0 V. (**a**) Ballistic model. Derived parameters: T_{c1} = 2.10 ± 0.01 K, $\Delta_1(0)$ = 85 ± 3 μeV, $\Delta C_1/C_1$ = 0.014 ± 0.001, $2\Delta_1(0)/k_BT_{c1}$ = 0.94 ± 0.04, T_{c2} = 0.252 ± 0.005 K, $\Delta_2(0)$ = 103 ± 4 μeV, $\Delta C_2/C_2$ = 1.5 ± 0.2, $2\Delta_2(0)/k_BT_{c2}$ = 9.5 ± 0.3, fit quality is R = 0.992; (**b**) Modified AB model [51]. Derived parameters: T_{c1} = 2.07 ± 0.03 K, $\Delta_1(0)$ = 144 ± 11 μeV, $\Delta C_1/C_1$ = 0.6 ± 0.2, $2\Delta_1(0)/k_BT_{c1}$ = 1.6 ± 0.2, R_{n1} = 3.9 ± 0.4 kΩ, T_{c2} = 0.33 ± 0.02 K, $\Delta_2(0)$ = 44 ± 8 μeV, $\Delta C_2/C_2$ = 0.20 ± 0.06, $2\Delta_2(0)/k_BT_{c2}$ = 3.1 ± 0.7, R_{n2} = 0.81 ± 0.15 kΩ, fit quality is R = 0.9965.

The same conclusion can be made for Sample 1 at V_g = 45 V (Fig. 5).

Preprints (www.preprints.org) | NOT PEER-REVIEWED | Posted: 27 September 2019 doi:10.20944/preprints201909.0307.v1

Peer-reviewed version available at *Nanomaterials* **2019**, *9*, 1554; doi:10.3390/nano9111554

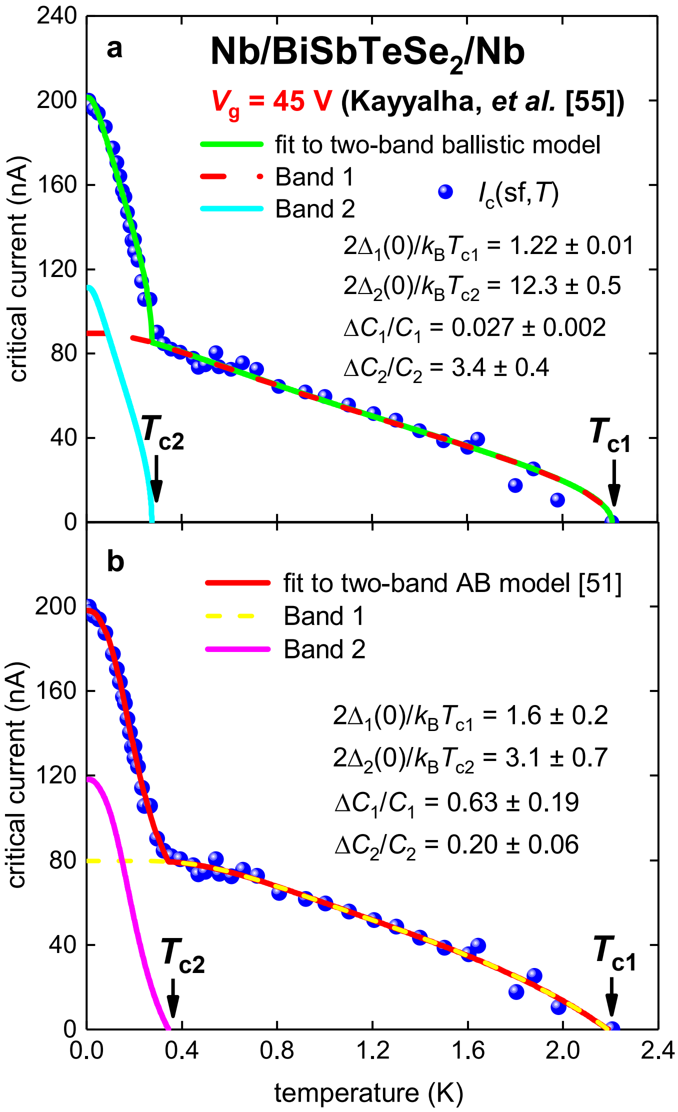

Figure 5. Experimental $I_c(\mathrm{sf},T)$ for Nb/BiSbTeSe$_2$-nanoribbon/Nb junction (Sample 1 [55]) at gate voltage $V_g = 45$ V. (**a**) Ballistic model. Derived parameters: $T_{c1} = 2.21 \pm 0.01$ K, $\Delta_1(0) = 116 \pm 4$ μeV, $\Delta C_1/C_1 = 0.027 \pm 0.002$, $2\Delta_1(0)/k_BT_{c1} = 0.94 \pm 0.04$, $T_{c2} = 0.274 \pm 0.006$ K, $\Delta_2(0) = 144 \pm 6$ μeV, $\Delta C_2/C_2 = 3.4 \pm 0.4$, $2\Delta_2(0)/k_BT_{c2} = 9.5 \pm 0.3$, fit quality is $R = 0.994$; (**b**) Modified AB model [51]. Derived parameters: $T_{c1} = 2.19 \pm 0.03$ K, $\Delta_1(0) = 176 \pm 13$ μeV, $\Delta C_1/C_1 = 0.63 \pm 0.09$, $2\Delta_1(0)/k_BT_{c1} = 1.9 \pm 0.2$, $R_{n1} = 3.5 \pm 0.3$ kΩ, $T_{c2} = 0.34 \pm 0.01$ K, $\Delta_2(0) = 47.6 \pm 8.7$ μeV, $\Delta C_2/C_2 = 0.30 \pm 0.08$, $2\Delta_2(0)/k_BT_{c2} = 3.06 \pm 0.70$, $R_{n2} = 630 \pm 110$ Ω, fit quality is $R = 0.998$.

3.3. Planar Nb/Bi$_2$Se$_3$/Nb junction [56]

In Fig. 6, temperature-dependent self-field critical currents, $I_c(\mathrm{sf},T)$, in Nb/Bi$_2$Se$_3$/Nb ($W = 1000$ nm, $L = 100$ nm) reported by Kurter *et al.* [56] is shown. For this junction 300 nm < ξ_c < 1,000 nm [56], and thus, the ballistic regime condition, $L \ll \xi_s$, is well satisfied.

There is a large difference between experimental data and the fit to ballistic model (Fig. 6). In addition, deduced parameters from the ballistic model fit have no physical interpretation. The fit to the modified AB model reveals parameters in expected ranges (Fig. 6).

Preprints (www.preprints.org) | NOT PEER-REVIEWED | Posted: 27 September 2019 doi:10.20944/preprints201909.0307.v1

Peer-reviewed version available at *Nanomaterials* **2019**, *9*, 1554; doi:10.3390/nano9111554

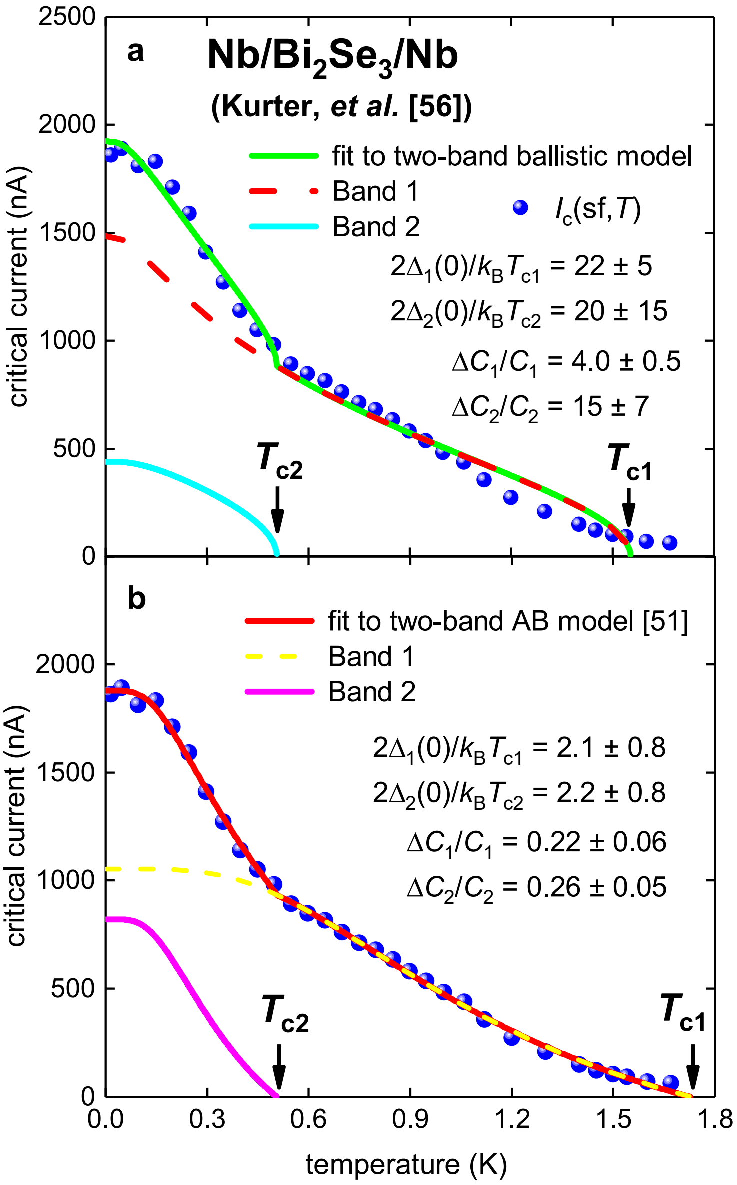

Figure 6. Experimental $I_c(sf,T)$ for Nb/Bi_2Se_2/Nb junction [56]. (**a**) Ballistic model. Derived parameters: $T_{c1} = 1.55 \pm 0.02$ K, $\Delta_1(0) = 1.44 \pm 0.35$ meV, $\Delta C_1/C_1 = 4.0 \pm 0.5$, $2\Delta_1(0)/k_BT_{c1} = 22 \pm 5$, $T_{c2} = 0.51 \pm 0.03$ K, $\Delta_2(0) = 427 \pm 329$ μeV, $\Delta C_2/C_2 = 15 \pm 7$, $2\Delta_2(0)/k_BT_{c2} = 20 \pm 15$, fit quality is $R = 0.994$; (**b**) Modified AB model [51]. Derived parameters: $T_{c1} = 1.73 \pm 0.05$ K, $\Delta_1(0) = 159 \pm 62$ meV, $2\Delta_1(0)/k_BT_{c1} = 2.1 \pm 0.8$, $\Delta C_1/C_1 = 0.22 \pm 0.06$, $R_{n1} = 240 \pm 100$ Ω, $T_{c2} = 0.51 \pm 0.03$ K, $\Delta_2(0) = 48 \pm 17$ meV, $2\Delta_2(0)/k_BT_{c2} = 2.2 \pm 0.8$, $\Delta C_2/C_2 = 0.26 \pm 0.05$, $R_{n2} = 92 \pm 33$ Ω. Fit quality is $R = 0.9991$.

There is a large difference between experimental data and the fit to ballistic model (Fig. 6). In addition, deduced parameters from ballistic model fit have no any physical interpretation. The fit to modified AB model reveals parameters in expected ranges (Fig. 6).

4. Discussion

One of the most important question which can be discussed herein, what is the origin for such dramatic incapability of ballistic model to analyze the self-field critical currents in S/DCM/S junctions. From the author's point of view the origin is the primary concept of the KO theory that $I_c(sf,T)$ in S/N/S junctions is:

$$I_c(sf,T) = \max_{\varphi}\big(I(\varphi,sf,T)\big) \tag{8}$$

Preprints (www.preprints.org) | NOT PEER-REVIEWED | Posted: 27 September 2019 doi:10.20944/preprints201909.0307.v1

Peer-reviewed version available at *Nanomaterials* **2019**, *9*, 1554; doi:10.3390/nano9111554

where φ is the phase difference between two superconducting electrodes of the junction. Despite this assumption is a fundamental conceptual point of the KO theory, there are no physically background or experimental confirmations that this assumption should be a true. In fact, the analysis of experimental data by a model within this assumption (we presented herein) shows that Eq. 8 is in remarkably large disagreement with experiment.

One of the simplest way to show that Eq. 8 is incorrect is to note that when the length of the junction, L, goes to zero, then for instance Eq. 5:

$$I_c(sf,T) = \lim_{L\to 0}\left(1.33\cdot\frac{e\cdot\Delta(T)}{\hbar}\cdot\frac{W}{\pi\cdot L}\right) \propto \lim_{L\to 0}\left(\frac{1}{L}\right) \to \infty. \tag{9}$$

Herein, the simplest available function [52] which was proposed for S/DCM/S junction in the Eq. 8, was chosen as an example. However, other proposed functions for Eq. 8 (for which we refer the reader to Ref. 11) have identical unresolved problem, because, as this was shown for about 100 weak-link superconductors [2-5,65], the limit should be (Eq. 1):

$$I_c(sf,T) = \lim_{L\to 0}\left(1.33\cdot\frac{e\cdot\Delta(T)}{\hbar}\cdot\frac{W}{\pi\cdot L}\right) = \frac{\phi_0}{\pi\cdot\mu_0}\cdot\left[\frac{ln\left(1+\sqrt{2}\cdot\kappa_c\right)}{\lambda_{ab}^3(T)}\cdot\left(\frac{\lambda_c(T)}{b}\cdot\tanh\left(\frac{b}{\lambda_c(T)}\right)\right)+\right.$$
$$\left.\frac{ln\left(1+\sqrt{2}\cdot\gamma(T)\cdot\kappa_c\right)}{\sqrt{\gamma(T)}\cdot\lambda_{ab}^3(T)}\left(\frac{\lambda_{ab}(T)}{a}\tanh\left(\frac{a}{\lambda_{ab}(T)}\right)\right)\right]\cdot(a\cdot b). \tag{10}$$

This means that the primary dissipation mechanism, which governs DC transport current limit in S/N/S is not revealed yet, but as we show herein it is irrelevant to achieving values within the primary concept of KO theory, which is Eq. 8.

It should be mentioned that Density Functional Theory (DFT) calculations [66,67] is one of unexplored to date powerful techniques, which can be used to reveal dissipation mechanism in S/DCM/S junctions.

5. Conclusions

In this paper $I_c(sf,T)$ data for S/DCM/S junctions were analyzed by applying two models: ballistic and modified Ambegaokar-Baratoff model. It was shown that ballistic model [9-11,53] cannot describe the self-field critical currents in S/DCM/S junctions. As a conclusion, there is a need that the ballistic model should be reexamined in terms of its applicability to describe dissipation-free self-field transport current in S/DCM/S junctions.

Funding: This research was funded by the State Assignment of Minobrnauki of Russia, theme "Pressure" No. AAAA-A18-118020190104-3, and by Act 211 Government of the Russian Federation, contract No. 02.A03.21.0006.

Conflicts of Interest: The funders had no role in the design of the study, in the collection, analyses, or interpretation of data, as well as in the writing of the manuscript, or in the decision to publish the results.

References

1. Hirsch, J.E.; Maple. M.B.; Marsiglio, F. Superconducting materials classes: Introduction and overview. *Physica C* **2015**, *514*, 1-8.
2. Talantsev, E.F. and Tallon, J.L. Universal self-field critical currents for thin-film superconductors. *Nature Communications* **2015**, *6*, 7820.
3. Talantsev, E.F.; Crump, W.P.; Tallon, J.L. Thermodynamic parameters of single-or multi-band superconductors derived from self-field critical currents. *Annalen der Physics* **2017**, *529*, 1700197.
4. Talantsev, E.F. and Crump, W.P. Weak-link criterion for pnictide and cuprate superconductors. *Superconductor Science and Technology* **2018**, *31*, 124001.
5. Talantsev, E.F.; Crump, W.P.; Tallon, J.L. Universal scaling of the self-field critical current in superconductors: from sub-nanometre to millimetre size. *Scientific Reports* **2018**, *7*, 10010.
6. Holm, R.; Meissner, W. Messungen mit Hilfe von flüssigem Helium. XIII. Kontaktwiderstand zwischen Supraleitern und Nichtsupraleitern (Measurements using liquid helium. XIII. Contact resistance between superconductors and non-superconductors). *Zeitschrift für Physik* **1932**, 74, 715-735.
7. Ambegaokar, V.; Baratoff, A. Tunneling between superconductors. *Phys. Rev. Lett.* **1963**, *10*, 486-489.
8. Ambegaokar, V.; Baratoff, A. Errata: Tunneling between superconductors. *Phys. Rev. Lett.* **1963**, *11*, 104.

Preprints (www.preprints.org) | NOT PEER-REVIEWED | Posted: 27 September 2019 doi:10.20944/preprints201909.0307.v1

Peer-reviewed version available at *Nanomaterials* **2019**, *9*, 1554; doi:10.3390/nano9111554

9. Kulik, I.O.; Omel'yanchuk, A.N. Contribution to the microscopic theory of the Josephson effect in superconducting bridges. *JETP Letters* **1975**, *21*, 96-97.
10. Kulik, I.O.; Omel'yanchuk, A.N. Properties of superconducting microbridges in the pure limit. *Sov. J. Low Temp. Phys.* **1977**, *3*, 459–462.
11. Kulik, I and A. Omelyanchouk, A. The Josephson effect in superconducting constructions: Microscopic theory. *Journal de Physique Colloques* **1978**, *39 (C6)*, C6-546-C6-547. 10.1051/jphyscol:19786245.
12. Lee, G. H. and Lee, H. J. Proximity coupling in superconductor-graphene heterostructures. *Rep. Prog. Phys.* **2018**, *81*, 056502.
13. Park, J.; *et al.* Short ballistic Josephson coupling in planar graphene junctions with inhomogeneous carrier doping. *Phys. Rev. Lett.* **2018**, *120*, 077701.
14. Takane, Y. and Imura, K.-I. Quasiclassical theory of the Josephson effect in ballistic graphene junctions. *J. Phys. Soc. Jpn.* **2012**, *81*, 094707.
15. Strickland, N.M.; *et al.* Nanoparticle additions for enhanced flux pinning in YBCO HTS films. *Current Applied Physics* **2008**, *8*, 372-375.
16. Talantsev, E.F.; *et al.* Critical current anisotropy for second generation HTS wires. *Current Applied Physics* **2008**, *8*, 388-390.
17. Chepikov, V.; *et al.* Introduction of $BaSnO_3$ and $BaZrO_3$ artificial pinning centres into 2G HTS wires based on PLD-GdBCO films. Phase I of the industrial R&D programme at SuperOx. *Superconductor Science and Technology* **2017**, *30*, 124001.
18. Paturi, P.; Malmivirta, M.; Hynninen, T.; Huhtinen, H. Angle dependent molecular dynamics simulation of flux pinning in YBCO superconductors with artificial pinning sites. *J. Phys.: Condens. Matter* **2018**, *30*, 315902.
19. Hänisch, J.; Iida, K.; Hühne, R.; Tarantini, C. Fe-based superconducting thin films—preparation and tuning of superconducting properties. *Superconductor Science and Technology* **2019**, *32*, 093001.
20. Qu, D.-X., *et al.* Onset of a two-dimensional superconducting phase in a topological-insulator – normal-metal $Bi_{1-x}Sb_x$/Pt junction fabricated by ion-beam techniques. *Phys. Rev. Lett.* **2018**, *121*, 037001.
21. Li, C.-Z. *et. al.* Bulk and surface states carried supercurrent in ballistic Nb-Dirac semimetal Cd_3As_2 nanowire-Nb junctions. *Phys. Rev. B* **2018**, *97*, 115446.
22. Reyren, N., *et al.* Superconducting interfaces between insulating oxides. *Science* **2007**, 317, 1196-1199.
23. Gozar, A., Logvenov, G., Fitting Kourkoutis, L., Bollinger, A.T., Giannuzzi, L.A., Muller, D.A., and Bozovic, I. High-temperature interface superconductivity between metallic and insulating copper oxides, *Nature* **2008**, *455*, 782-785.
24. Di Castro, D.; Balestrino, G. Superconductivity in interacting interfaces of cuprate-based heterostructures *Supercond. Sci. Technol.* **2018**, *31*, 073001.
25. Qing-Yan, W.; *et al.* Interface-induced high-temperature superconductivity in single unit-cell FeSe films on $SrTiO_3$. *Chin. Phys. Lett.* **2012**, *29*, 037402.
26. Zhang, W.-H.; *et al.* Direct observation of high-temperature superconductivity in one-unit-cell FeSe films. *Chin. Phys. Lett.* **2014**, *31*, 017401.
27. Ge, J.F.; *et al.* Superconductivity above 100 K in single-layer FeSe films on doped $SrTiO_3$. *Nature Materials* **2015**, *14*, 285-289.
28. Zhang, H.M.; *et al.* Detection of a superconducting phase in a two-atom layer of hexagonal Ga film grown on semiconducting GaN(0001). *Phys. Rev. Lett.* **2015**, *114*, 107003.
29. Xing, Y.; *et al.* Quantum Griffiths singularity of superconductor-metal transition in Ga thin films. *Science* **2015**, *350*, 542-545.
30. Navarro-Moratalla, E.; *et al.* Enhanced superconductivity in atomically thin TaS_2. *Nat. Comms.* **2016**, *7*, 11043.
31. Yankowitz, M.; Chen, S.; Polshyn, H.; Watanabe, K.; Taniguchi, T.; Graf, D.; Young, A.F.; Dean, C.R. Tuning superconductivity in twisted bilayer graphene. *Science* **2019**, *363*, 1059-1064.
32. Lucignano, P.; Alfè, D.; Cataudella, V.; Ninno, D.; Cantele, G. The crucial role of atomic corrugation on the flat bands and energy gaps of twisted bilayer graphene at the "magic angle" $\theta\sim1.08°$. *Phys. Rev. B* **2019**, *99*, 195419.
33. Fête, A.; Rossi, L.; Augieri, A.; Senatore, C. Ionic liquid gating of ultra-thin YBa2Cu3O7-x films. *Appl. Phys. Lett.* **2016**, *109*, 192601.

34. Fête, A.; Senatore, C. Strong improvement of the transport characteristics of $YBa_2Cu_3O_{7-x}$ grain boundaries using ionic liquid gating. *Scientific Reports* **2017**, *8*, 17703.
35. Paradiso, N.; Nguyen, A.-T.; Kloss, K.E.; Strunk, C. Phase slip lines in superconducting few-layer $NbSe_2$ crystals. *2D Materials* **2019**, *6*, 025039.
36. Guo, J.G.; *et al.* Quasi-two-dimensional superconductivity from dimerization of atomically ordered $AuTe_2Se_{4/3}$ cubes. *Nature Communications* **2017**, *8*, 871.
37. Pan, J.; *et al.* Enhanced superconductivity in restacked TaS_2 nanosheets. *J. Am. Chem. Soc.* **2017**, *139*, 4623.
38. Ma, Y.; *et al.* Unusual evolution of B_{c2} and T_c with inclined fields in restacked TaS_2 nanosheets. *npj Quantum Materials* **2018**, *3*, 34.
39. Desrat, W.; *et al.* Superconducting Ga/GaSe layers grown by van der Waals epitaxy. *Mater. Res. Express* **2018**, *5*, 045901.
40. Liu, C.; *et al.* Two-dimensional superconductivity and topological states in $PdTe_2$ thin films. *Physical Review Materials* **2018**, *2*, 094001.
41. Peng, J.; *et al.* Disorder enhanced superconductivity toward TaS_2 monolayer. *ACS Nano* **2018**, *12*, 9461-9466.
42. De La Barrera, S.C.; *et al.* Tuning Ising superconductivity with layer and spin-orbit coupling in two-dimensional transition-metal dichalcogenides. *Nature Communications* **2018**, *9*, 1427.
43. Liao, M., *et al.* Superconductivity in few-layer stanene. *Nature Physics* **2018**, *14*, 344-348.
44. Wu, Y.; *et al.* Dimensional reduction and ionic gating induced enhancement of superconductivity in atomically thin crystals of 2H-$TaSe_2$. *Nanotechnology* **2019**, *30*, 035702.
45. Alidoust, M.; Willatzen, M.; Jauho, A.-P. Symmetry of superconducting correlations in displaced bilayers of graphene. *Phys. Rev. B* **2019**, *99*, 155413.
46. Lucignano, P.; Alfè, D.; Cataudella, V.; Ninno, D.; Cantele, G. The crucial role of atomic corrugation on the flat bands and energy gaps of twisted bilayer graphene at the "magic angle" $\theta \sim 1.08°$. *arXiv* **2019**, arXiv:1902.02690
47. Talantsev, E.F.; Mataira, R.C.; Crump, W.P. Classifying superconductivity in Moiré graphene superlattices. *arXiv* **2019**, arXiv:1902.07410v2.
48. Rhodes, D.; *et al.* Enhanced superconductivity in monolayer T_d-$MoTe_2$ with tilted Ising spin texture. *arXiv* **2019**, arXiv:1905.06508.
49. Yang, H.; Gao, Z.-Q.; Wang, F. Effect of defects in superconducting phase of twisted bilayer graphene. *arXiv* **2019**, arXiv:1908.09555v2.
50. Talantsev, E.F.; Crump, W.P.; Island, J.O.; Xing, Y.; Sun, Y.; Wang, J.; Tallon, J.L. On the origin of critical temperature enhancement in atomically thin superconductors. *2D Materials* **2017**, *4*, 025072.
51. Talantsev, E.F.; Crump, W.P.; Tallon, J.L. Two-band induced superconductivity in single-layer graphene and topological insulator bismuth selenide. *Supercond. Sci. & Technol.* **2018**, *31*, 015011.
52. Titov, M. and Beenakker, C. W. J. Josephson effect in ballistic graphene. *Phys. Rev B* **2006**, *74*, 041401(R).
53. Calado, V.E.; *et al.* Ballistic Josephson junctions in edge-contacted graphene. *Nature Nanotech.* **2015**, *10*, 761–764.
54. Borzenets, I.V.; *et al.* Ballistic graphene Josephson junctions from the short to the long junction regimes *Phys. Rev. Lett.* **2016**, 117, 237002.
55. Kayyalha, M., *et al.* Anomalous low-temperature enhancement of supercurrent in topological-insulator nanoribbon Josephson junctions: Evidence for low-energy Andreev bound states. *Phys. Rev. Lett.* **2019**, *122*, 047003.
56. Kurter, C.; Finck, A.D.K.; Hor, Y.S.; Van Harlingen, D.J. Evidence for an anomalous current–phase relation in topological insulator Josephson junctions. *Nature Communications* **2015**, *6*, 7130.
57. Gross, F.; *et al.* Anomalous temperature dependence of the magnetic field penetration depth in superconducting UBe_{13}. *Zeitschrift für Physik B Condensed Matter* **1986**, *64*, 175-188.
58. Natterer, F.D.; Ha, J.; Baek, H.; Zhang, D.; Cullen, W.G.; Zhitenev, N.B.; Kuk, Y.; Stroscio, J.A. Scanning tunneling spectroscopy of proximity superconductivity in epitaxial multilayer graphene. *Phys Rev. B* **2016**, *93*, 045406.
59. Talantsev, E.F. Classifying induced superconductivity in atomically thin Dirac-cone materials. *Condensed Matter* **2019**, *4*, 83.
60. Dyson, F. A meeting with Enrico Fermi. *Nature* **2004**, *427*, 297.
61. Piantadosi, S. T. One parameter is always enough. *AIP Adv.* **2018**, *8*, 095118.

62. Jang, S. and Kim, E. Short ballistic Josephson coupling in micrometer-long tantalum/graphene/tantalum junction. *Current Applied Physics* **2019**, *19*, 436-439.
63. Carbotte, J.P. Properties of boson-exchange superconductors. *Rev. Mod. Phys.* **1990**, *62*, 1027-1157.
64. Nicol, E.J. and Carbotte, J.P. Properties of the superconducting state in a two-band model. *Phys. Rev. B* **2005**, *71*, 054501.
65. Talantsev, E. F. Evaluation of a practical level of critical current densities in pnictides and recently discovered superconductors. *Superconductor Science and Technology* **2019**, *32*, 084007.
66. Mackinnon, I.D.R., Talbot, P.C. and Alarco, J.A. Phonon dispersion anomalies and superconductivity in metal substituted MgB_2. *Computational Materials Science* **2017**, *130*, 191-203.
67. Alarco, J.A., Talbot, P.C. and Mackinnon, I.D.R. Identification of superconductivity mechanisms and prediction of new materials using Density Functional Theory (DFT) calculations. *Journal of Physics: Conference Series* **2018**, *1143*, 012028.